PASJ: Publ. Astron. Soc. Japan **45**, 477–485 (1993)

One-Dimensional Imaging with the Waseda FFT Radio Telescope

Junichi NAKAJIMA, Eiichiro OTOBE, Kazuhiko NISHIBORI,
Hiromi KOBAYASHI, Naoki TANAKA, and Tomohiro SAITOH
Astrophysics, Department of Pure and Applied Physics,
Graduate School of Science and Engineering,
Waseda University, 4-1 Okubo 3-chome, Shinjuku-ku, Tokyo 169

Naoki WATANABE, Yoshitaka ARAMAKI, and Tomoyuki HOSHIKAWA
Astrophysics, Department of Electronics and Communication,
Graduate School of Science and Engineering,
Waseda University, 4-1 Okubo 3-chome, Shinjuku-ku, Tokyo 169

Kuniyuki ASUMA
Souka Highschool, 3-1 Aoyagi 5-chome, Souka, Saitama 340
and
Tsuneaki DAISHIDO
Astrophysics, Department of Science, School of Education, Waseda University,
6-1 Nishi-waseda 1-chome, Shinjuku-ku, Tokyo 169

(Received 1992 November 17; accepted 1993 January 29)

Abstract

A sixty-four-element fast Fourier transform (FFT) type radio interferometer has been constructed at Waseda University. Using eight east-west elements, eight one-dimensional beams were formed. The analog phase errors in the baseband signals of 64 channels were measured by fringe observations, and were corrected by a digital processor. Images of two radio sources were obtained in transit observation, when they passed the fixed eight fan-beams. This is the real-time one-dimensional imaging of eight pixels. The present image forming technique could be a basis for two-dimensional imaging. We report the frontend system and its performance in the observation.

Key words: Fast Fourier transform — Imaging — Radio interferometer

1. Introduction

Large-field sensitive radio telescopes have been developed to search for transient radio objects, such as radio supernovae and radio bursts, in stellar systems (Daishido et al. 1984). The present paper describes the spatial fast-Fourier transform (FFT) type radio telescope at Waseda University, being an equally-spaced, maximum redundant, two-dimensional (2D) array in an 8×8 configuration. Although it is only partially operating at 10.65 GHz, the completed system having 64 beams in the northern hemisphere is expected to provide maps having 0.1° angular resolution and a sensitivity of 50 mJy. The beams are formed by a newly-developed "Digital Lens" (complex amplitude equalizer + 2D FFT processor), with the array's overall size being 20 m × 20 m (Daishido et al. 1991). The Digital Lens was designed under a parallel, pipelined architecture operating at 20 MHz (Iwase et al. 1988).

Fringe observations of radio sources until 1991 November were previously reported (Nakajima et al. 1992a,b), and were also carried out in 1991 December to measure the instrumental phase error. After the phase equalization, eight one-dimensional (1D) beams were formed.

2. Radio Telescope System

2.1. *System Frontend*

Sixty-four identically-designed frontend elements comprise 2.4-m diameter cassegrain antennas and high mobility electron transistor (HEMT) receivers; figure 1 is schematic diagram of a single element. In this transit radio telescope, elevation steering is accomplished with common shafts that are synchronously-controlled by a servo motor. Being fixed during observations, the telescope scans the sky using the Earth's rotation. The entire 20 m × 20 m configuration has an angle of about 15.5° with the north-south direction. The observable sky is 40° in zenith distance, and the entire northern hemisphere

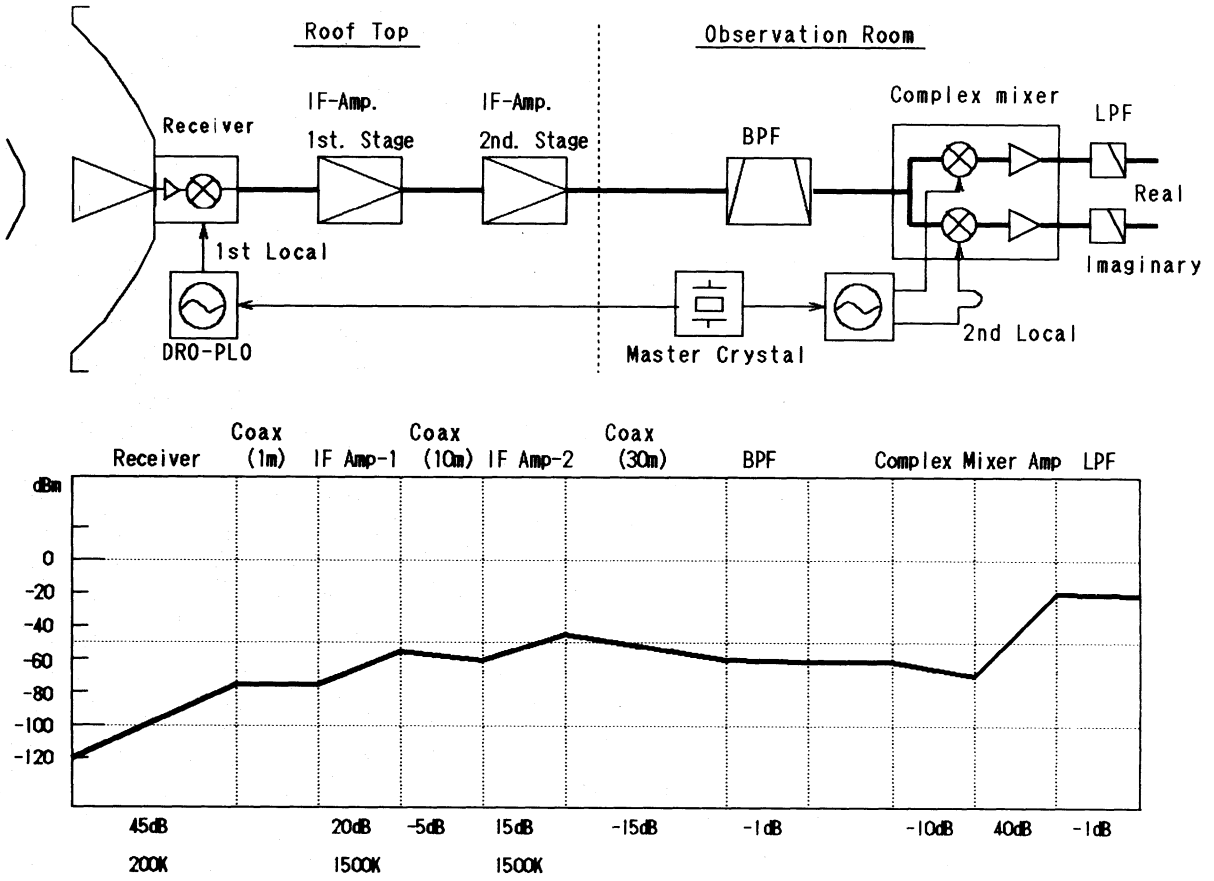

Fig. 1. One-element schematic diagram of the frontend, the IF, and the local signal components of the 64-element Waseda FFT interferometer. The corresponding signal level, gain, and noise temperature of the components are also indicated (lower).

($\delta \geq 0°$) is covered.

The 2.4-m diameter cassegrain antenna, with a pyramidal horn at secondary focus, was designed by Otobe et al. (private communication), and has a half power beam width (HPBW) of 0.8°. The 64 HEMT receivers achieve a 45-dB gain and a 200 K noise temperature in typical operation. They were originally designed for a Broadcasting Satellite (BS) frequency at 11.5 GHz, but were modified to 10.65 GHz by Nishibori et al. (1993) for radio astronomy. For phase-locked local oscilators (PLO), we used new compact DRO-locked PLOs developed by Nihon Tsushinki Co. Ltd.. Figure 2 shows a photo of frontend unit, the receiver, the PLO, and the first stage IF amplifier.

2.2. *IF System*

Down converted 1-GHz IF signals from the receivers are transmitted 50 m in length by 75-Ω coaxial cables. This relatively high IF frequency at an attenuation of 20 dB is recovered by a two-stage amplifier unit. Figure 3 shows a photo of the second stage IF amplifier array. The IF signal is filtered in the observation room to remove the interference, and is then converted to a baseband, complex double-side band (DSB) signal of −10 to +10 MHz by the complex mixer units . The accuracy of these units' orthogonality is within ±1°. The baseband signal passes through a low-pass filter for anti-aliasing and is connected to the Digital Lens. The system temperature $T_{\rm sys}$, typically 250 K, is calculated from the antenna temperature $T_{\rm A}$, the RF and IF components noise temperature T_i, and the gain G_i, i.e.,

$$T_{\rm sys} = T_{\rm A} + \sum_n \frac{T_i}{\prod_i G_i}. \quad (1)$$

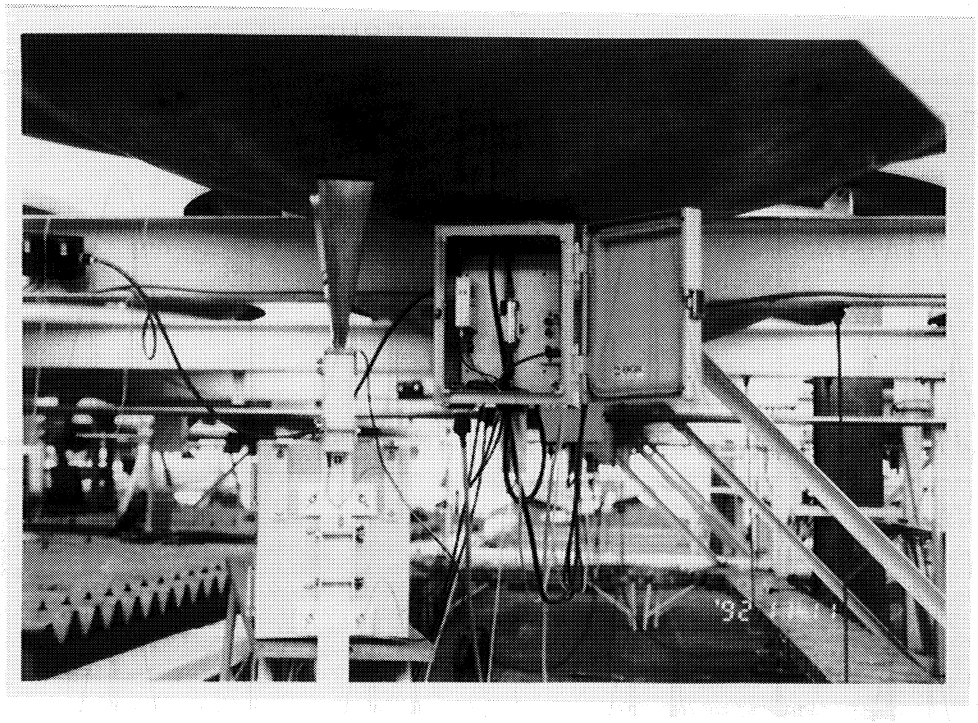

Fig. 2. Photo of the frontend unit, receiver, PLO, first stage IF amplifier, and DC supply circuit as attached to the base of the cassegrain dish. The mounted receiver is adjustable at the secondary focus.

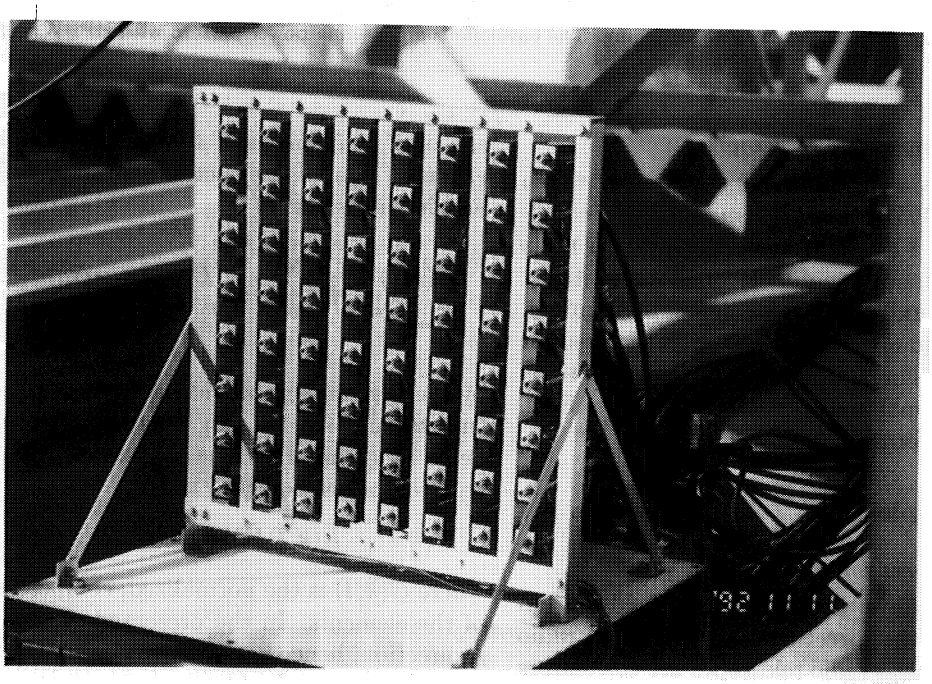

Fig. 3. Photo of the IF amplifier-array, comprising 1.0-GHz second IF amplifiers which form an 8×8 array at the intermediate point of the transmission line.

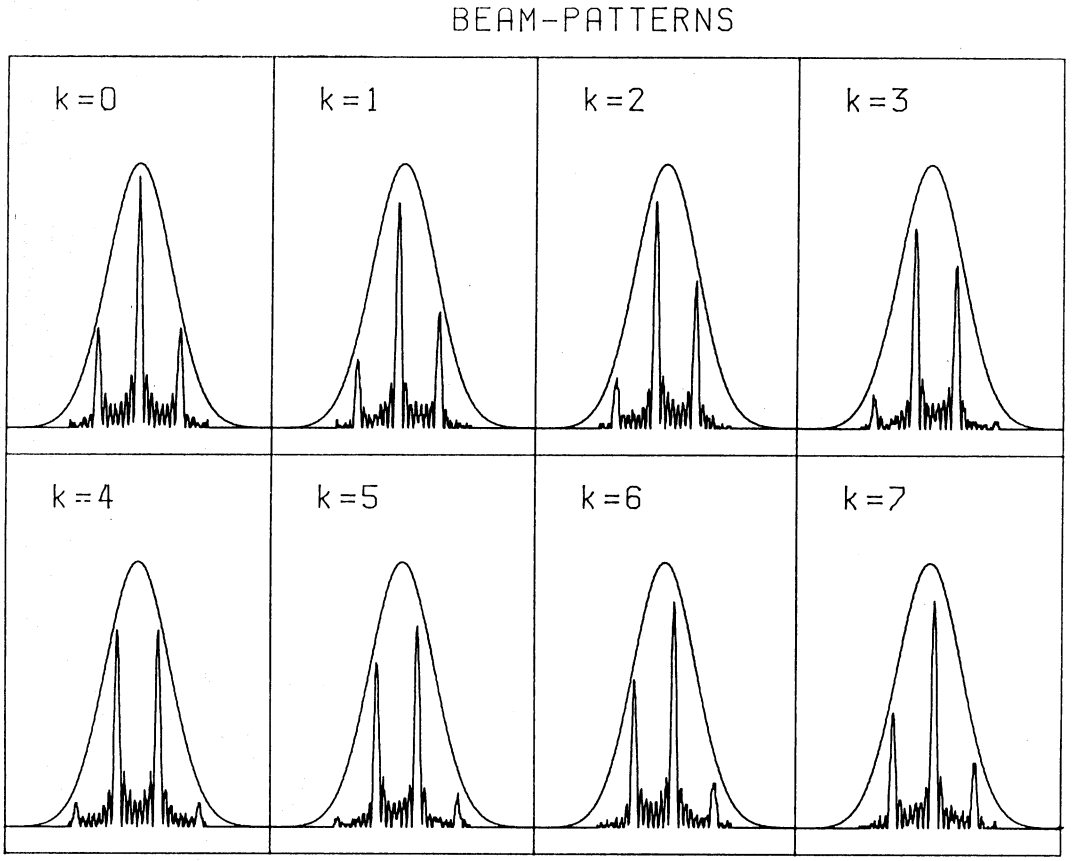

Fig. 4. Theoretical beam patterns with no switching. The envelope is an antenna power pattern with HPBW= 0.°8.

2.3. *Digital Lens (Imaging Processor)*

The Digital Lens is a digital imaging processor which consists of complex A/D converters and complex equalizers, X- and Y-axis FFT, and power integration units (Iwase et al. 1988). In our one-dimensional observations, only one X-axis FFT unit (8-complex signals) is required. The rest of the X- and all Y-axis FFT units are used for fringe observations. For a 2-s power integration time, 4×10^8 data are accumulated by the Digital Lens. Each output pixel has the form of a 32-bit integer.

3. Imaging Principle

3.1. *Fourier Transform for Sky Imaging*

The Fourier transform of an electric field on an aperture plane gives the directional amplitude of radio sources. Fourier synthesis radio telescopes use correlators for the Fourier transform to obtain the fine angular structure of such sources. On the other hand, a wide-field, real-time imaging interferometer has been developed by Daishido et al. (1984). To obtain a two-dimensional image of $N \times N$ pixels of the sky, $N \times N$ equally-spaced elements sample the electric field of $E(m\Delta x, n\Delta y)$. The Fourier transform of

$$\tilde{E}(k,l) = \frac{1}{N^2} \sum_{m=0}^{N-1} \sum_{n=0}^{N-1} E(m\Delta x, n\Delta y) e^{-i2\pi \frac{k}{N} m} e^{-i2\pi \frac{l}{N} n}, \tag{2}$$

by the Digital Lens provides a representation in k, l space (momentum space). In practice, the sampled electric fields are limited by the individual elements, with the received power being

$$P(k,l) = \tilde{E}(k,l)\tilde{E}^*(k,l)G(k,l)\ , \tag{3}$$

where $G(k,l)$ is the normalized, composite beam pattern of the elements. In the presented system, $N = 8$ in the k direction, hence equation (3) becomes

$$P(k) = \tilde{E}(k)\tilde{E}^*(k)G(k,l). \tag{4}$$

Figure 4 shows the theoretical beam patterns of the eight elements. The spatial resolution of the fan-beams in the k-direction is $\lambda/(7\Delta x) = 0.°084$ (3.′4).

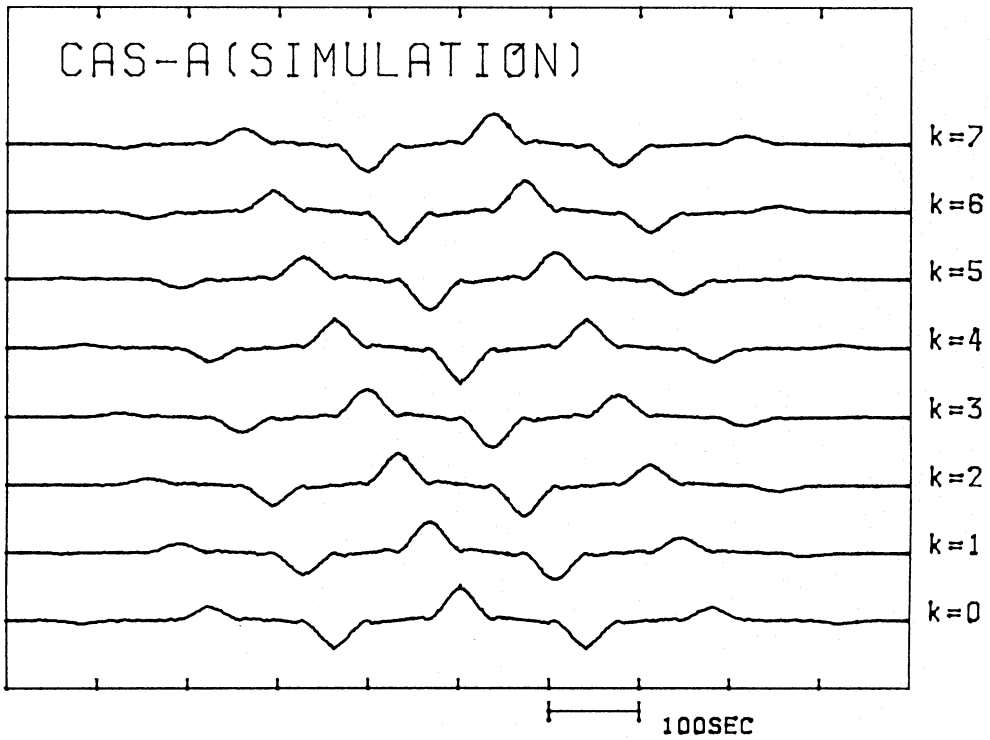

Fig. 5. Theoretical beam patterns with beam switching. The subtracted (negative) beam is indicated. The source declination is $\delta = 58°$, Cas A.

3.2. *Beam Switching*

If the receivers are temperature-controlled and operated under limited man-made radio interferency, observation with the beam patterns in figure 4 is possible. However, our receivers are operated at ambient temperature and the telescope is located in an urban area with radio interefernce, thereby necessitating removal of the DC drifts and such interference. Consequently, the beam switching technique is used in which the switching speed is faster than the time scale of the receivers' gain fluctuation and the change of external interference. Under these conditions, only astronomical signals are correlated, and sensitive astronomical observations are possible. The process is expressed as

$$P(k) = G(k)[\tilde{E}(k)\tilde{E}^*(k) - \tilde{E}_\xi(k)\tilde{E}^*_\xi(k)] \ , \qquad (5)$$

where

$$\tilde{E}_\xi(k) = e^{i\xi}\tilde{E}(k) \ , \ \tilde{E}^*_\xi(k) = e^{i\xi}\tilde{E}^*(k) \ . \qquad (6)$$

An adjustable phase rotation ξ is applied to digitized data. In the present experiment, 180° ($\xi = \pi$) switching was employed. Simulated beam patterns are shown in figures 5 and 6, and respectively correspond to a point source observation of $\delta = 58°$ (Cas A) and $\delta = 22°$ (Tau A).

4. Phase Correction and Beam Forming

4.1. *Fringe Observation*

The phase at the input of the FFT stage must be adjusted for beam forming. The time scale of the instrumental phase fluctuations are several days and frequent adjustments are not necessary. To obtain the instrumental phase differences, including the path differences occurring in cassegrain systems, a pair of receivers are correlated and the fringes of far-field celestial radio sources are used. The phase measuring fringe observation with the large array and the Digital Lens were described by Nakajima et al. (1992b). Fringe patterns for various baseline pairs were used to determine the phase errors via Young's two-slit interferometric method (Asuma et al. 1991). In this method, the instrumental phase error is obtained by the fringe shift on the image plane.

Here, a quick procedure was developed to measure the phase errors by the fringe shift on the time domain. The fringe pattern obtained between two neighboring east-west elements is given as

$$P_{i,i+1}(k,\phi,\psi) = \frac{4A_iA_{i+1}E^2(0\Delta x)}{N^2}\cos\left(2\pi\frac{k}{N} - \phi - \psi_{i,i+1}\right) , \qquad (7)$$

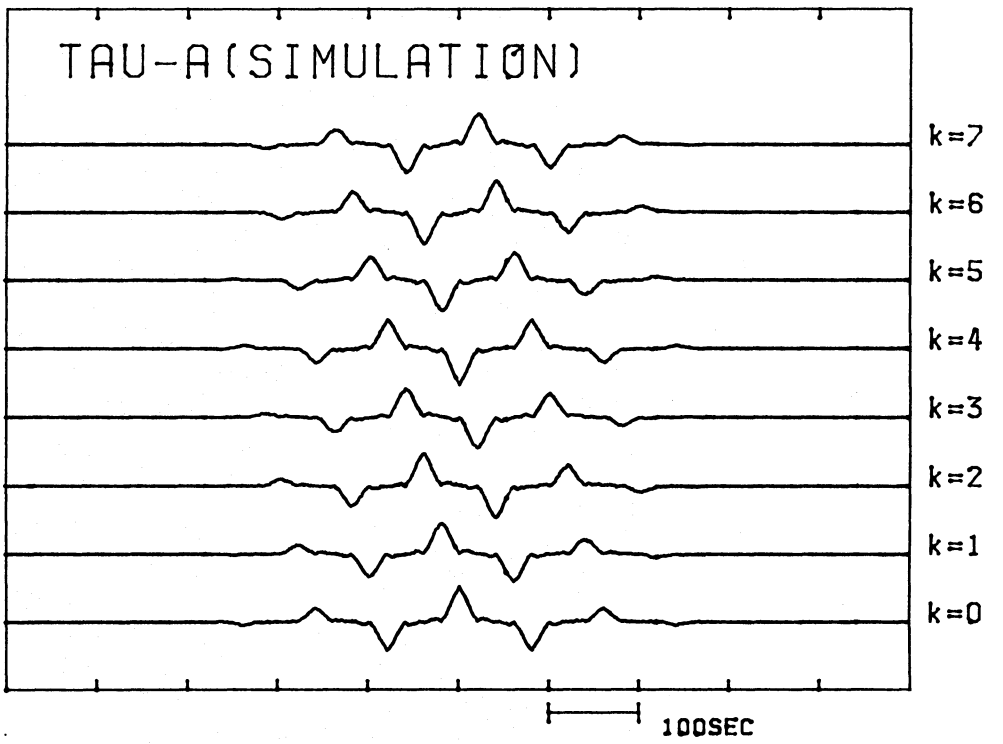

Fig. 6. Theoretical beam patterns with beam switching. The subtracted (negative) beam is indicated. The source declination is $\delta = 22°$, Tau A.

where $i = 0, 1, 2, \cdots, 7$, and ϕ is the phase due to the source direction, and $\psi_{i,i+1}$ is the instrumental phase error between an i and i+1 element. Seven minimum baselines exist for the current 1D, eight-element observation. The corresponding seven fringe patterns $P_{01}, P_{12}, \cdots P_{67}$ were used to determine the phase errors $\psi_{01}, \psi_{12}, \cdots \psi_{67}$. For the phase calibration, source declination δ and integration time τ determine the resolution of the fringe phase. A higher resolution is achieved at a higher source declination angle, such for the source Cas A ($\delta = 58°$). For example, the resolution $d\phi/dt$ is

$$\frac{d\phi}{dt} = 360 \times \frac{\Delta x}{\lambda}\omega_e \cos(\delta_{\text{Cas A}}) = 1.^\circ 3\ \text{s}^{-1}, \tag{8}$$

where the angular speed of the earth ω_e is 0.727 $\times 10^{-4}$ rad s^{-1}, the projected east-west baseline Δx is 2.628 m, and the wavelength of the center frequency λ is 2.817×10^{-2} m. As a result, the fringe rate with $\tau = 2$ s has an in-phase step accuracy of 2.°6.

4.2. Phase Error Measurement

Phase error measurement and beam formation are described in this section. The seven observed fringe patterns are $P_{i,i+1}(k, \phi, \psi_{i,i+1})$. As an example, we use the direction output of $k = 0$, with the other fringe outputs being used to improve S/N. The result is then compared to a theoretical fringe pattern $P(0, \phi, 0)$, which is maximized using the actual transit time to the source. ψ is measured by the delay or advance duration (t_s) from the theoretical fringe maximum. The time t_s is measured between $P_{i,i+1}(0, \phi, \psi)$ and $P(0, \phi, 0)$. The phase difference between two neighboring elements is therefore

$$\psi_{i,i+1} = \frac{d\phi_{\text{source}}}{dt} t_s\ . \tag{9}$$

Figure 7 depicts the fringe observation mode. To determine the seven $\psi_{i,i+1}$ parameters, observation of all fringes were simultaneously made. Analog power dividers are used in the baseband signal. The phase error due to divider installation can be neglected. The eastern most element No. 0 is defined as the phase origin, and the phase to other elements $\psi_{0,k}$ is

$$\psi_{0,k} = \sum_{n=0}^{k} \psi_{n,n+1} \quad (-179° < \psi \leq 180°). \tag{10}$$

Table 1 summarizes the result of the initial fringe phase measurement for each element.

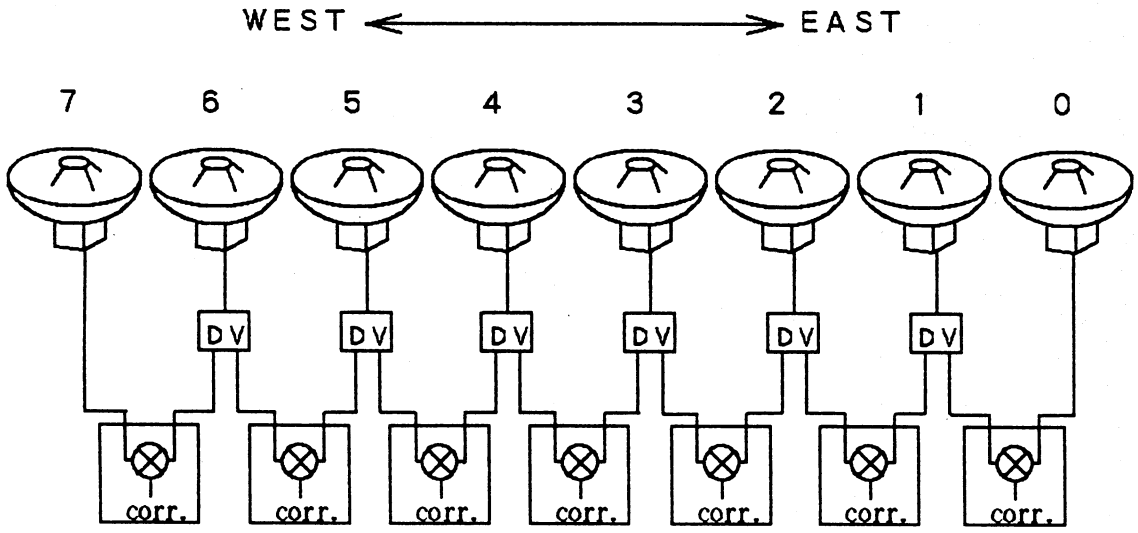

Fig. 7. Schematic of the fringe observation setup for element 0–7 to measure the phase error. The baseband signals are distributed by the analog dividers (DV).

Table 1. Summary of fringe phase measurement.

Element	0	1	2	3	4	5	6	7
phase $\psi_{i,i+1}$	65°	−25°	167°	−86°	34°	−77°	43°	—
phase $\psi_{0,i}$	—	65°	40°	−133°	121°	155°	78°	121°

4.3. Phase Adjustment Process

The complex amplitude correction to remove the phase and amplitude error in the i-th element is $(1/A_i)e^{-\psi_{0,i}}$. The differences in the amplitude gain A_i over the element are within a maximum of ±3 dB; thus the amplitude parameter was disregarded since we did not want to suppress the element gain in the first experiment. Image forming without gain correction slightly increases the sidebeam level, yet this does not seriously affect the imaging (Asuma et al. 1991). The complex amplitude equalizer coefficeients are preset by $e^{-\psi_{0,i}}$.

4.4. One-Dimensional Imaging

Observations were carried out on the strong radio sources of Cas A and Tau A from 1991 December 5–11, with figures 8 and 9 respectively showing the one-dimentional differential image for the eight elements. The lower-declination source passes faster, and so it passes the beams in a shorter time. Five days of continuous monitoring revealed that the beam patterns were sustained in winter under stable temperature and humidity conditions. Changes in the environment, such as rain, gradually distorted the beams. No obvious mutual coupling occurred between the elements.

4.5. Beam Patterns

The raw data obtained from the Digital Lens for the observed sources are shown in figures 8 and 9, and indicate that these sources can be considered as being point sources. Compared with the corresponding theoretical beam patterns in figures 5 and 6, it is remarkable how much the side beams of the observed data are suppressed. The main beam levels are higher than would be expected due to no amplitude corrections. In the present observations, the pointing errors were ±0.°1 in the East-West and ±0.°2 in the North-South directions. Such errors in pointing introduce a wide HPBW of the composite beam patterns and lower its gain, as well as shifting the beam's peak position. Thus, a symmetrical beam pattern does not appear at $k = 0$. A coefficient η_p was therefore introduced into the sensitivity calculation to give the pointing completeness. Moon transit observations are used to

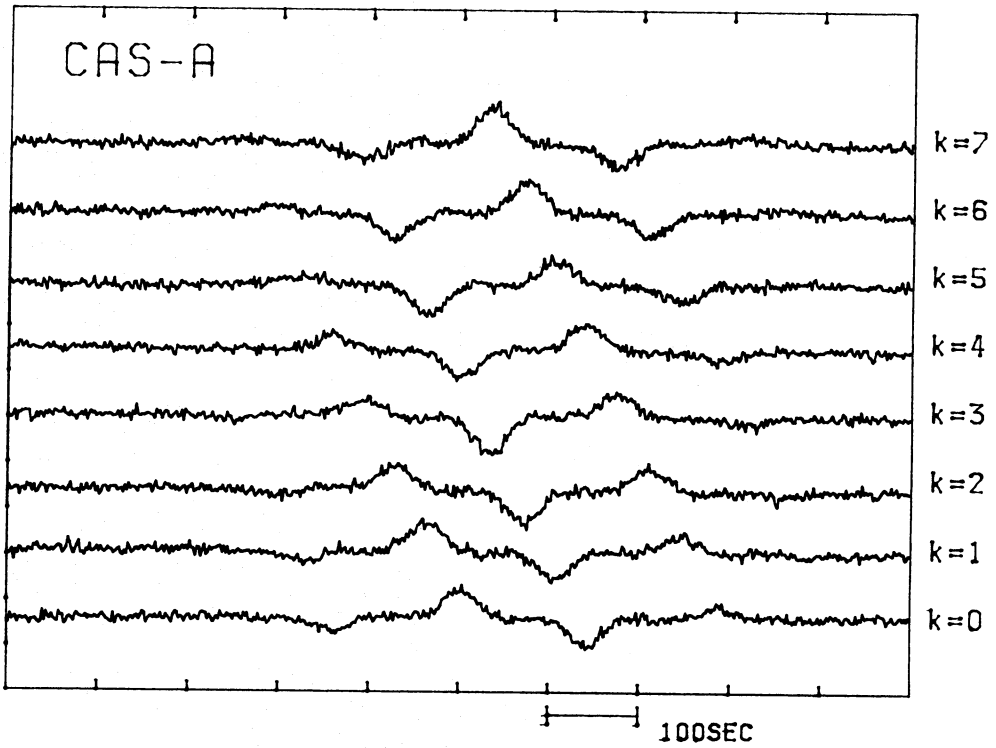

Fig. 8. One-dimensional images of Cas A. The outputs correspond to the eight directions.

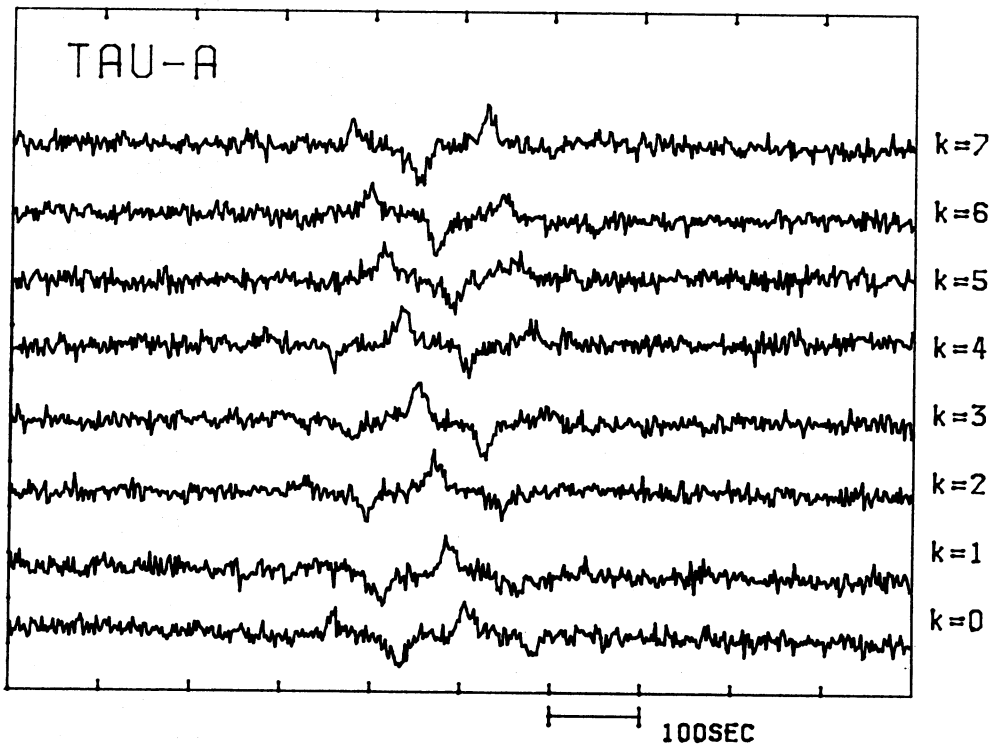

Fig. 9. One-dimensional images of Tau A. The outputs correspond to the eight directions.

Table 2. Observation parameters.

Source	Cas A	Tau A
Date	1991 Dec 5	1991 Dec 6
R.A.	$23^h21^m7^s$	$5^h34^m6^s$
Decl.	58°33′48	22°01′0
Elevation	65.°8	76.°0
Flux [10 GHz]* Jy	520	537
Source Size	4′ × 4′	3′.3 × 4′.0
Fringe Frequency ($\times 10^{-3}$ Hz) [$\Delta x = 2.628$ m]	3.539	6.300
$\Delta S_{\min}$ [1σ] Jy	40	45

* Baars 1973.

measure the cassegarin main beam directivity of the eight-elements. By using the beam offsets and the beam patterns, $\eta_p = 0.82$ for the field center was calculated.

4.6. *Sensitivity*

The minimum sensitivity $\Delta S_{\min}$ of the present system is calculated using

$$\Delta S_{\min} = \frac{2kK_sT_{sys}}{\eta_p\eta_e A\sqrt{\eta_f \Delta f \tau}} \approx 13 \text{ Jy}, \quad (11)$$

where the system temperature T_{sys} is 250 K, the bandwidth Δf is 20 MHz, and the effective bandwidth is $\eta_f \Delta f$ (the difference from the rectangular passband). The efficiency η_f (= 0.80) is based upon the anti-aliasing filter and digital filter inside the processor. Boltzmann's constant k is 1.38×10^{-23} JK^{-1}, the aperture A is 36.2 m^2, the aperture efficiency η_e is 0.64, the integration time τ is 2.048 s, and the sensitivity constant K_s is 2.0 for a 180° beam switching observation.

When the calculated $\Delta S_{\min}$ is compared with the observed value given in table 2, they differ by a factor of 3 . This discrepancy may possibly be caused by a misspointing of the composite beam in the North-South direction. The η_p (= 0.82) for the field center of the composite beam decreases at the offset position. The existence of high-noise temperature elements may also influence the sensitivity. These problems can be mitigated by adjusting the antenna pointing and replacing faulty components. The eight outputs from the Digital Lens, however, are time independent. This is useful since we can shift the data from other directions and add them; there by improving the minimum sensitivity by a factor of $\sqrt{8}$.

5. Conclusion

We have completed the installation of the sixty-four element Waseda FFT interferometer and subsequently conducted beam forming using eight of its elements. Resultant phase measurements enabled the beam forming and radio source observations. The mentioned pointing problem is being resolved, and will be presented separately.

This project was funded by the Toray Science Foundation and was supported by the Waseda University Grant for Special Research Projects, the Scientific Research Fund of Japanese Ministry of Education, Science and Culture (01400006), and the Yamada Science Foundation.

References

Asuma, K., Iwase, S., Nishibori, K., Nakajima, J., Otobe, E., Tsuchiya, A., Watanabe, N., and Daishido, T. 1991, in *Radio Interferometory: Theory, Techniques, and Applications, IAU Colloq. No. 131*, ed. T. J. Cornwell and R. A. Perley (Astronomical Society of the Pacific, San Francisco), p. 90.

Baars Jacob, W. M. 1973, in *IEEE Trans. Antenna Propagation*, Vol. AP-21, No. 4, (IEEE press), p. 461.

Daishido, T., Asuma, K., Nishibori, K., Nakajima, J., Yano, M., and Otobe, E. 1991, in *Radio Interferometory: Theory, Techniques, and Applications, IAU Colloq. No. 131*, ed. T. J. Cornwell and R. A. Perley (Astronomical Society of the Pacific, San Francisco), p. 86.

Daishido, T., Ohkawa, T., Yokoyama, T., Asuma, K., Kikuchi, H., Nagane, K., Hirabayashi, H., and Komatsu, S. 1984, in *Indirect Imaging*, ed. J. A. Roberts (Cambridge University Press, Cambridge), p. 81.

Iwase, S., Okita, T., Yamazaki, T., Daishido, T., and Asuma, K. 1988, *Denshi Tushin Gakkai Ronbunshi*, Vol. J71-A No. 2, p. 320. (in Japanese) [English Translation: *Electronics and Comunications in Japan*, Part 3 : Fundmental Electronic Science (Scripta Technica, Inc./Wiley)].

Nakajima, J., Otobe, E., Asuma, K., and Daishido, T. 1992a, in *Frontiers of X-Ray Astronomy, Proceeding of 28th Yamada Conference*, ed. Y. Tanaka and K. Koyama (Universal Academy Press, Tokyo), p. 713.

Nakajima, J., Otobe, E., Nishibori, K., Watanabe, N., Asuma, K., and Daishido, T. 1992b, *Publ. Astron. Soc. Japan*, **44**, L35.

Nishibori, K., Otobe, E., Yano, M., Nakajima, J., Watanabe, N., Daishido, T., Asuma, K., Musashiya, T., Hoshino, T., and Abe, Y. 1993, in *Proceeding of International Workshop for Reference Frame Establishment and Technical Development in Space Geodesy*, IRIS93 Tokyo, Communication Research Laboratory, p. 125–128.